Article

Identification of ACE2 as the Entry Receptor for Two Novel European Bat Merbecoviruses

Chengbao Ma[1,#], Chen Liu[1,#], Qing Xiong[1], Xiao Yu[1], Yuanmei Chen[1], Junyu Si[1], Peng Liu[1], Fei Tong[1], Meiling Huang[1], Huan Yan[1,*]

[1] State Key Laboratory of Virology, Institute for Vaccine Research and Modern Virology Research Center, College of Life Sciences, TaiKang Center for Life and Medical Sciences, Wuhan University, Wuhan, Hubei, 430072, China.

[#] These authors contributed equally to this work.

[*] Correspondence: huanyan@whu.edu.cn

Address: Luojia Mountain, Wuchang District, Wuhan 430072, China

Abstract

The unknown identity of the entry receptors utilized by many coronaviruses has significantly impeded our comprehensive understanding of these important pathogens. We recently reported an unexpected usage of angiotensin-converting enzyme 2 (ACE2), instead of Dipeptidyl peptidase-4 (DPP4), for cellular entry by NeoCoV and PDF-2180, close relatives of MERS-CoV that infect African bats. However, the presence and distribution of other ACE2-using merbecoviruses remain enigmatic. In this study, through sequence and structural analyses, we predicted that two newly discovered merbecoviruses infecting European Pipistrellus bats (*Pipistrellus nathusii*), namely MOW-15-22 and PnNL2018B, may also utilize ACE2 as their receptors. Functional profiling of 103 ACE2 orthologues from a variety of mammals confirmed that several ACE2 from bats efficiently facilitate the entry of MOW-15-22 and PnNL2018B. Conversely, no binding or entry signals for both viruses were detected when assessing seven DPP4 orthologues from humans, hedgehogs, and bats. Characterization of Pteronotus davyi (P.dav) ACE2 mediated entry of MOW-15-22 reveals a significant exogenous protease dependence, which can be dose-dependently neutralized by soluble P.dav ACE2 recombinant protein and a broadly neutralizing S2-targeting antibody. Verification of the previously reported critical ACE2 determinants for NeoCoV recognition reveals that MOW-15-22 and PnNL2018B displayed a glycan-independent binding mode with significantly altered interaction details. This study sheds light on two additional ACE2-using merbecoviruses circulating among European bats and underscores the potential zoonotic risk associated with these viruses.

Keywords: Bats, Receptor, MOW-15-22, PnNL2018B, ACE2, Merbecoviruses, Host tropism

Introduction

The COVID-19 pandemic has underscored the critical need for close monitoring the zoonotic spillover of animal coronaviruses, particularly those originating from bat species (Chiroptera), known as the primary natural reservoirs for at least hundreds of α and β-coronaviruses[1-8]. Notably, the three high pathogenic human coronaviruses, SARS-CoV, SARS-CoV-2, and MERS-CoV, all belong to the β-coronaviruses genus[5,9,10]. MERS-CoV, classified under the merbecoviruses subgenus, is the causative agent for the Middle East respiratory syndrome with a case-fatality rate of 36%, which caused sporadic transmission since its outbreak in 2012 [11]. Although dromedary camels have been well documented as intermediate host of MERS-CoV, the evolutionary origin of this virus remains unclear and has been linked to potential recombinations in bat merbecoviruses [12-17].

The viral receptor is a key host factor for viral entry, determining tissue tropism, host range, and transmission efficiency of viruses[18-21]. Thus far, ACE2 and DPP4 have been widely acknowledged protein receptors for β-coronaviruses. both are engaged by the C-terminal domain (or domain B) of subunit 1 (S1-CTD) of viral spike proteins[22,23]. Typically, ACE2 is considered the primary entry receptor for sarbecoviruses, whereas DPP4 is thought to mediate entry for many merbecoviruses, although uncharacterized receptor usage has been found in viruses from both subgenus[5,24-31]. However, recent discoveries have challenged these notions. NeoCoV and PDF-2180, two close relatives of MERS-CoV found in African bats, employ a novel interaction mode to recognize ACE2 as their functional receptors, revealing a receptor usage promiscuity among merbecoviruses[32]. While these two viruses exhibit limited efficiency in using human ACE2 (hACE2), a single mutation (e.g., T510F) in the receptor binding motif (RBM) enhances their ability to enter human cells. Moreover, NeoCoV and PDF-2180 display a broad ACE2 recognition spectrum across various mammals, underscoring a relatively high zoonotic risk[32,33].

Nonetheless, the receptors for many merbecoviruses, including hedgehog coronaviruses (EriCoVs) such as HKU31, as well as several other bat coronaviruses like HKU5, MOW-15-22, and PN-βCoV remain elusive[29,34-36]. Previous studies have suggested that HKU5 and HKU31 may not use DPP4 or ACE2 as their receptors, leaving their entry receptor identities to be determined.

61 MOW-15-22 and PN-βCoV are two bat merbecoviruses recently identified in *P. nathusii* bats, a bat
62 species commonly found in Europe[35,36]. To avoid confusion, we designated a specific virus of
63 PN-βCoV (Betacoronavirus sp. isolate BtCoV/P.nathusii/NL/2018-403.3) as PnNL2018B in this
64 study since both viruses are β-CoVs infecting the same host. MOW-15-22 was discovered in the
65 Mosco region, while the PnNL2018B was identified in bats residing in the Netherlands with
66 complete genome sequenced, although its relative VM314 (defined based on a sequence fragment in
67 its RNA-dependent RNA polymerase) has been reported as early as in 2010[37]. Notably, some studies
68 have proposed that DPP4 may serve as the entry receptor for MOW-15-22 and PnNL2018B based on
69 molecular docking analyses.

70 In this study, we demonstrated that two recently reported European merbecoviruses,
71 MOW-15-22 and PnNL2018B, with considerable genetic differences with the previously identified
72 ACE2-using merbecoviruses, also utilize bat ACE2 rather than DPP4 as their functional receptors
73 through a series of cellular and biochemical experiments. Our findings suggest that the diversity of
74 ACE2-using merbecoviruses may be broader than previously recognized, raising concerns about the
75 potential human emergence of these viruses.

76

77 **Results**

78 **Phylogenetic and structural analyses suggest ACE2 usage by MOW-15-22 and PnNL2018B**

79 Recently, two novel bat merbecoviruses with complete genome sequenced, MOW-15-22 and
80 PN-βCoV (designated PnNL2018B in this study), were independently reported by research teams in
81 Russia and Netherlands[35,36] (**Fig. 1a**). Both viruses were discovered in *P. nathusii*, a bat species
82 inhabiting a wide range of Europe and undertakes a seasonal long-distance migration, usually from
83 northeast to southwest Europe (**Fig. 1b**)[38,39]. In our quest to identify receptors for representative
84 merbecoviruses, we noticed these two viruses form a distinct clade and exhibited an unknown
85 receptor usage. At the complete-genome level, MOW-15-22 and PnNL2018B share less genetic
86 similarity with the African bat coronaviruses NeoCoV and PDF-2180 but show greater genetic
87 homology with a Italian bat merbecovirus (Hsavll/Italy/206645-40/2011) and a DPP4-using virus
88 HKU25[35,40](**Fig. 1c**). However, their RBD sequences from these viruses cluster with the ACE2-using
89 NeoCoV/PDF-2180 and an Asian hedgehog virus HKU31 (**Fig. 1d**). Aligning of equivalent
90 sequences based on the NeoCoV receptor binding motif (RBM) reveals a relatively variable region

with low conservation, signifying uncertainty regarding receptor usage **(Fig. 1e)**. Importantly, the MOW-15-22 and PnNL2018B possess two insertions at the putative RBM compared to other merbecoviruses, potentially significantly influencing receptor interactions. Notably, the AlphaFold-predicted RBD structures of MOW-15-22 and PnNL2018B more closely resemble the ACE2-utilizing merbecoviruses NeoCoV and PDF-2180 in view of the presence of an helix region within the RBM, albeit with elongated putative receptor binding loops (**Fig. 1f**). Simplot analysis queried by MERS-CoV genome sequences demonstrates that the RBD regions of MOW-15-22 and PnNL2018B display lower similarity to MERS-CoV compared to the DPP4-using HKU4 (**Fig. 1g**). Collectively, these data suggest potential ACE2 usage by MOW-15-22 and PnNL2018B, eventhough they are phylogenetic distant from NeoCoV and PDF-2180 at the whole-genome level.

Multi-species ACE2 usage spectrum of MOW-15-22 and PnNL2018B

To determine whether MOW-15-22 and PnNL2018B utilize ACE2 as their receptors, we conducted a series of cell-based experiments to evaluate the functionality of various ACE2 orthologue in facilitating viral RBD binding and pseudovirus entry. As the complete genome sequences or coding sequences of ACE2 and DPP4 orthologues from *P. nathusii* are currently unavailable, we utilized a well-characterized receptor library consisting of 103 ACE2 and 7 DPP4 orthologues from 52 bats and 53 non-bat mammals to comprehensively assess RBD binding and pseudovirus entry efficiency[33]. These assays were carried out in 293T cells transiently transfected with plasmids expressing the receptors, all of which were previously confirmed to be properly expressed.. Our findings indicate that MOW-15-22 pseudovirus entry occurred in cells expressing bat ACE2 from P. par, P. dav, L. bor, and several other bat species, while the the PnNL2018B pseudovirus entry was supported by bat ACE2 from L. bor, N. hum, P. pip, and several other bat species (**Fig. 2a)**. Notably, in contrast to NeoCoV and PDF-2180, which exhibit a broad potential host tropism, both MOW-15-22 and PnNL2018B were incapable of efficiently utilizing ACE2 from non-bat mammals **(Fig. 2b).** Although we lack ACE2 binding data from the host species P. nat, we observe efficient RBD binding of MOW-15-22 in cells expressing two ACE2 orthologues from the *Pteronotus* genus (P. dav and P. par) (**Fig. 2a**). Furthermore, no binding or entry signal was detected in cells expressing human ACE2 and several DPP4 orthologues from the indicated species (**Fig. 2c-g**). It's important to note that the observed inconsistency between RBD binding and viral entry is a phenomenon commonly observed

121 in other coronaviruses, including NeoCoV/PDF-2180 and SARS-CoV/SARS-CoV-2[32,41]. One
122 possible explanation for this phenomenon is that RBD binding is dynamic, whereas pseudotype entry
123 is a cumulative event. Consequently, some receptors with kinetic features of fast association and fast
124 dissociation can mediate efficient entry but may not exhibit strong binding in end-point binding
125 assays. Indeed, the relative entry efficiency is also greatly influenced by the presence of exogenous
126 trypsin (**Fig. 2h-j**), which is believed to lower the energy barrier and facilitate viral entry[42]. Therefore,
127 ACE2 orthologues that are less efficient in supporting viral binding, such as L. bor ACE2, exhibited
128 significantly higher dependence on the presence of TPCK-treated trypsin (**Fig. 2j**).
129

130 **Characterization of bat ACE2-mediated entry of novel ACE2-using merbecoviruses**

131 We proceeded to characterize the functionality of representative bat ACE2 in mediating the
132 infection of these European merbecoviruses. A live-cell immunofluorescence-based RBD-hFc
133 binding assay demonstrated that P.dav and P.par ACE2 efficiently facilitated the RBD binding of
134 MOW-15-22 (**Fig. 2a**). Flow cytometry was subsequently conducted to confirm specific RBD
135 binding supported by the ACE2 orthologues from P.dav and P.par, with human ACE2 (hACE2) as a
136 negative control **(Fig. 3a).** Binding kinetics between MOW-15-22 RBD and P.dav or human ACE2
137 were analyzed using the Biolayer Interferometry (BLI). In general, P.dav ACE2 exhibited rapid
138 association with MOW-15-22 RBD. However, the dissociation of P.dav ACE2 from MOW-15-22
139 RBD was also fast compared to the P.pip ACE2-NeoCoV RBD complex, resulting in a KD of
140 approximately 10 nM (**Fig. 3b)**. By contrast, no binding signal was detected between human ACE2
141 and MOW-15-22 RBD (**Fig. 3c)**.

142 We further investigated the viral spike-mediated cell-cell membrane fusion assisted by different
143 ACE2 orthologues. The two novel ACE2-using viruses lack furin cleavage sites at the S1/S2 junction
144 (**Fig. S1**). Consequently, MOW-15-22 exhibited a prominent trypsin-dependent membrane fusion
145 phenotype in bat ACE2-expressing cells, as was similarly observed in NeoCoV and PDF-2180[32] (**Fig.**
146 **3d-e**). Notably, although L.bor ACE2 failed to support detectable MOW-15-22 RBD binding, its
147 expression and interaction with MOW-15-22 spike proteins induced a considerable amount of
148 membrane fusion in the presence of exogenous trypsin (**Fig. 3d-e**). We also investigated whether the
149 entry of ACE2-using viruses could be neutralized by interfering with the viral-receptor interaction.
150 We demonstrated that viral entry could be efficiently inhibited by recombinant soluble ACE2 or

151 MOW-15-22 RBD-hFc fusion proteins (**Fig. 3f, and S2)**. Additionally, we evaluated the potency of
152 MERS-CoV RBD-specific nanobodies and pan-β-CoV broadly neutralizing S2 antibodies targeting
153 the stem helix (S2P6) or the S2' cleavage site/fusion peptide (76E1) (**Fig. 3g-i**)[43,44]. However, neither
154 the MERS-CoV RBD-specific nanobodies nor S2P6 cross-reacted with MOW-15-22 or PnNL2018B
155 to show inhibitory activity. This might be attributed to the discrepancy of equivalent sequences from
156 these viruses in the S2P6 epitope compared with that of SARS-CoV-2 (**Fig. 3j**). Nevertheless,, 76E1
157 maintained its potency to neutralize the entry of these viruses due to the conservation of the critical
158 residues in this epitope across these merbecoviruses (**Fig. 3k**).
159
160 **Glycan-independent ACE2 recognition by MOW-15-22**
161 Previous investigations into the interaction between P.pip ACE2 and NeoCoV/PDF-2180 revealed a
162 unique glycan-dependent ACE2 binding mode[32]. Four molecular determinants, designated A to D,
163 located in the binding interface in ACE2 were demonstrated crucial for species-specific ACE2
164 recognition. Among them, determinants A and C carry glycosylation sites, while determinants B and
165 D are characterized by critical residues capable of forming salt bridges in P.pip ACE2 (**Fig. 4a**).
166 Probably due to the RBM sequence variation, molecular docking did not provide a convincing
167 interaction model for MOW-15-22 and P.dav ACE2 complex **(Fig. S3)**. Nevertheless, sequence
168 analysis of P.dav and P.par ACE2 indicated that P.dav ACE2 shares similar residues with NeoCoV
169 within these determinants, while P.par contains unfavorable residues in determinants B and C for
170 NeoCoV interaction. Therefore, several P.dav and P.par ACE2 mutants carrying theoretically
171 unfavorable residues, as indicated in previous studies based on NeoCoV, were generated to test the
172 involvement of these determinants in MOW-15-22 receptor recognition **(Fig. 4b)**.
173 Immunofluorescence and immunoblotting assays indicated that these mutants were expressed at
174 similar levels **(Fig. 4c,e)**. As expected, introducing unfavorable residues within these determinants
175 impaired NeoCoV RBD binding and pseudovirus entry. However, all these mutants maintained their
176 receptor functionality for MOW-15-22, including P.par-T56I ACE2, which lost glycosylation in both
177 A and C determinants **(Fig.4d-e)**. Unfavorable residues in determinant D are crucial in restricting
178 human ACE2 from supporting NeoCoV binding and entry. However, hACE2 carrying the N338D
179 mutation remains incapable of supporting MOW-15-22 or PnNL2018B entry **(Fig. S4)**. These results
180 indicate that the ACE2 recognition mode utilized by these European ACE2-using merbecoviruses

differs considerably from NeoCoV and PDF-2180, which displayed a glycan-independent manner.

Discussion

Coronaviruses exhibit remarkable variations in RBD sequences, resulting in diverse receptor usage modes across different viruses[45]. Within the same genus or subgenus, coronaviruses often share very similar RBD core structures, but differences in receptor binding motifs (loops) can result in entirely different receptor usage[22,32,46]. Conversely, phylogenetically distant coronaviruses can convergently employ the same receptor during evolution. For example, receptor APN is shared by many alphacoronaviruses and deltacoronaviruses[46-49], while ACE2 serves as a common receptor for alphacoronaviruses and many sarbecoviruses[5,24,25,30]. Recently, we discovered ACE2 usage in merbecoviruses, NeoCoV and PDF-2180, expanded the ACE2 receptor usage to the third subgenus of coronaviruses[32].

The discovery of ACE2 usage in bat merbecoviruses closely related to MERS-CoV highlights the potential zoonotic risk associated with these viruses. Consequently, it becomes imperative to explore the global prevalence and distribution of ACE2-using merbecoviruses. Through scrutiny into RBM sequences and functional screening of receptor usage based on a mammalian ACE2 library, we identified two European bat coronaviruses, MOW-15-22 and PnNL2018B, as novel ACE2-utilizing merbecoviruses, despite prior studies proposing DPP4 usage based on molecular docking. Our findings strongly emphasize the need to verify *in silico* receptor usage predictions through functional binding and entry experiments, especially for coronaviruses with promiscuous receptor usage patterns.

In a previous report, we demonstrated that NeoCoV and PDF-2180 employ a glycan-assisted ACE2 interaction mode. However, glycan appears dispensable for ACE2 recognition by MOW-15-22 and PnNL2018B. Furthermore, it seems that the two other ACE2 determinants established by NeoCoV and PDF-2180 do not apply to the two European ACE2-using merbecoviruses. These discrepancies suggest a variation in ACE2 interaction mode. Revealing the cryo-EM structure of the viral MOW-15-22 RBD-Bat30 ACE2 complex in future studies could provide critical insights into the receptor recognition details of these viruses.

Compared to NeoCoV/PDF-2180, the two European ACE2-using merbecoviruses exhibit a narrow ACE2 recognition spectrum, with only a few bat ACE2 receptors facilitating pseudotyped

211 virus entry or RBD binding. It is likely that both viruses have a strict preference for their hosts'
212 ACE2 receptors. Unfortunately, we were unable to test the ACE2 or DPP4 orthologues from this host
213 species due to the unavailability of the complete genome sequence of *P. nathusii*. Neither of these
214 viruses could use hACE2 based on their current sequences, and it remains unknown whether these
215 viruses can acquire efficient recognition of hACE2 through point mutations in their RBM, akin to
216 T510F in NeoCoV[32]. Overall, these two viruses exhibited lower spillover potential compared to
217 NeoCoV and PDF-2180 at the receptor entry level.

218 The ACE2 usage was convergently established by different coronaviruses despite remarkable
219 differences in their RBD structures. This ACE2 preference likely provides certain evolutionary
220 advantages in transmission, as exemplified by the highly transmissible SARS-CoV-2 omicron strain
221 [50,51]. However, a recent study reported that PnNL2180B (PN-βCoV) primarily exhibits intestinal
222 tropism in its natural host, suggesting a potential fecal-oral route used by these viruses[36]. Given that
223 airbrone transmission is the major route of all known ACE2-using human coronaviruses, it is
224 important to investigate whether tissue tropism and transmission route changes when ACE2-using
225 viruses jump from bats to humans.

226 Previous studies have revealed potential recombination events during the evolution of
227 merbecoviruses, shedding light on the evolutionary history of MERS-CoV and related viruses[27,32].
228 Additionally, hypotheses have been proposed that ACE2-utilizing merbecoviruses might have arisen
229 as a result of recombination between ancestral viruses of bats and hedgehogs. However, thus far, we
230 have not detected any evidence of ACE2 usage by testing a hedgehog coronaviruses HKU31[29,32,52].
231 These observations raise interesting questions regarding the evolution trajectory of merbecoviruses
232 and whether ACE2 or DPP4 receptor usage is the more ancestral trait for these viruses.

233 Our study significantly contributes to the understanding of ACE2-utilizing merbecoviruses by
234 identifying and characterizing two novel ACE2-using merbecoviruses, expanding the known
235 geographic distribution of these viruses to Europe in addition to Africa. The discovery of
236 MOW-15-22 and PnNL2018B underscores the likelihood of many other yet-to-be-discovered
237 ACE2-utilizing merbecoviruses, suggesting a potentially broader distribution than currently
238 acknowledged Therefore, a comprehensive and expanded monitoring effort is essential to proactively
239 detect and respond to potential outbreaks of ACE2-using merbecoviruses in humans. In-depth
240 research on these viruses is warranted to provide valuable insights into their pathogenicity and

241 transmission abilities. Although we demonstrated that bat ACE2 recombinant proteins or broadly
242 neutralizing antibodies can effectively block the entry of these viruses, future efforts of developing
243 specific antibodies and vaccines are necessary to achieve better protection. Additionally, it is
244 paramount to prepare effective antiviral drugs and vaccines to mitigate the risk of potential outbreaks
245 caused by ACE2-using merbecoviruses.
246
247 **Materials and methods**
248
249 **Cell lines**
250 HEK293T (CRL-3216) and I1-Hybridoma (CRL-2700) cell line was acquired from the American
251 Type Culture Collection (ATCC). These cells were maintained in Dulbecco's Modified Eagle
252 Medium (DMEM, Monad, China) supplemented with 1% PS (Penicillin/Streptomycin) and 10%
253 Fetal Bovine Serum. The I1-Hybridoma cell line, which produces a neutralizing antibody targeting
254 the VSV glycoprotein (VSVG), was cultured in Minimum Essential Medium (MEM) with Earles's
255 balances salts and 2.0 mM of L-glutamine (Gibico) and 10% FBS. All cell lines were cultured at
256 37°C with 5% CO_2 and underwent regular passage every 2-3 days.
257
258 **Plasmids and vectors**
259 Plasmids expressing wild-type (WT) or mutated bats ACE2 orthologues were constructed by
260 inserting human codon-optimized sequences with/without specific mutations into a lentiviral transfer
261 vector (pLVX-EF1a-Puro, Genewiz) with C-terminus 3×Flag tags
262 (DYKDHD-G-DYKDHD-I-DYKDDDDK). For the expression of non-bat mammalian ACE2,
263 human codon-optimized sequences of all ACE2 from non-bat mammals were cloned into a vector
264 (pLVX-IRES-zsGreen) with a C-terminal Flag tag (DYKDDDDK). For pseudovirus production,
265 human codon-optimized spike sequences of MOW-15-22 (USL83011.1), PnNL2018B
266 (WDE20340.1), SARS-CoV-2 (YP_009724390.1) carrying D614G mutation, MERS-CoV
267 (YP_009047204.1), HKU4 (AWH65899), NeoCoV (AGY29650.2) and HKU31 (QGA70692.1)
268 were cloned into the pCAGGS vector with C-terminal deletions (13-15aa) for improving the
269 pseudovirus assembly efficiency. For the expression of recombinant CoVs RBD-hFc fusion proteins,
270 plasmids were constructed by inserting NeoCoV RBD (380-585aa), MOW-15-22 RBD (360-610aa),

271 PnNL2018B RBD (361-606aa) coding sequences into the pCAGGS vector containing an N-terminal
272 CD5 secretion signal peptide (MPMGSLQPLATLYLLGMLVASVL) and a C-terminal hFc tag or
273 hFc-twin-strep tandem tags for purification and detection. Plasmids expressing soluble bat ACE2
274 ectodomain proteins were generated by integrating *Pteronotus davyi* sequences (18-738 amino acids)
275 into the pCAGGS vector, which included an N-terminal CD5 secretion signal peptide and a
276 C-terminal twin-strep-3 × Flag tag
277 (WSHPQFEKGGGSGGGSGGSAWSHPQFEKGGGRSDYKDHDGDYKDHDIDYKDDDDK).
278

279 **Protein expression and purification**

280 HEK293T cells were transfected with corresponding plasmids using GeneTwin reagent (Biomed,
281 TG101-01). Subsequently, the culture medium of the transfected cells was replaced with the SMM
282 293-TII Expression Medium (Sino Biological, M293TII) 4-6 hours post-transfection, and the
283 protein-containing supernatant was collected every three days for 2-3 batches. All recombinant
284 RBD-hFc proteins were purified using Pierce Protein A/G Plus Agarose (Thermo Scientific, 20424).
285 In general, hFc-fused proteins were captured by the Agarose, washed with wash buffer (100 mM
286 Tris/HCl, pH 8.0, 150 mM NaCl, 1 mM EDTA), eluted using the Glycine buffer (100 mM in H_2O,
287 pH 3.0), and immediately neutralized with 1/10 volume of 1M Tris-HCI, pH 8.0 (15568025, Thermo
288 Scientific). Proteins with twin-strep tag were purified using Strep-Tactin XT 4Flow high-capacity
289 resin (IBA, 2-5030-002), washed by wash buffer, and then eluted with buffer BXT (100 mM
290 Tris/HCl, pH 8.0, 150 mM NaCl, 1 mM EDTA, 50 mM biotin). All eluted proteins were
291 concentrated using Ultrafiltration tubes, buffer-changed to PBS, and stored at -80℃. Protein
292 concentrations were determined by the Omni-Easy Instant BCA Protein Assay Kit (Epizyme,
293 ZJ102).
294

295 **RBD-hFc live-cell binding assays**

296 The coronavirus RBD-hFc recombinant proteins were diluted in DMEM at indicated concentrations
297 and incubated with HEK293T cells expressing different ACE2 for 30 mins at 37℃ at 36 hours
298 post-transfection. Subsequently, cells were washed once with Hanks' Balanced Salt Solution (HBSS)
299 and incubated with either 1 μg/mL of Alexa Fluor 488-conjugated goat anti-human IgG (Thermo
300 Fisher Scientific; A11013) or DyLight 594-conjugated goat anti-human IgG (Thermo Fisher

301 Scientific; SA5-10136) diluted in HBSS/1% BSA for 1 hour at 37°C. After another round of washing
302 with HBSS, the cell nuclei were stained with Hoechst 33342 (1:10,000 dilution in HBSS) for 30
303 mins at 37°C. The images were captured using a fluorescence microscope (MI52-N). The relative
304 fluorescence intensities (RFU) of the stained cells were determined by a Varioskan LUX Multi-well
305 Luminometer (Thermo Scientific). For flow cytometry analysis, HEK293T cells transiently
306 expressing the indicated ACE2 orthologues were detached using 5 mM EDTA/PBS at 36 hours
307 post-transfection. These cells were washed twice with cold PBS and incubated with MOW-15-22 or
308 PnNL2018B RBD-hFc-twin-strep proteins at indicated concentrations at 4°C for 30 minutes.
309 Following this, cells were incubated with Alexa Fluor 488-conjugated goat anti-human IgG to stain
310 the RBD (Thermo Fisher Scientific; A11013) at 4°C for 1 hour. The cells were then fixed with 4%
311 PFA, permeabilized with 0.25% Triton X-100, blocked with 1% BSA/PBS at 4°C, and then
312 incubated with mouse antibody M2 (Sigma-Aldrich, F1804) diluted in PBS/1% BSA for 1 hour at
313 4°C, followed by incubation with Alexa Fluor 647-conjugated goat anti-mouse IgG (Thermo Fisher
314 Scientific; A32728) diluted in 1% BSA/PBS for 1 hour at 4°C. For all samples, 10,000
315 ACE2-expressinglive cells (gated based on Flag-fluorescence intensity and SSC/FSC) were analyzed
316 using a CytoFLEX Flow Cytometer (Beckman).
317
318 **Biolayer interferometry (BLI) binding assay**
319 Protein binding kinetics was analyzed using BLI assays with the Octet RED96 instrument
320 (Molecular Devices) following the manufacturer's instructions. Generally, RBD-hFc recombinant
321 proteins were diluted into the (20 μg/mL) and immobilized on the Protein A (ProA) biosensors
322 (ForteBio, 18-5010), and then incubated with bat ACE2-ectodomain proteins, two-fold serial-diluted
323 starting from 1000 nM, in a kinetic buffer (PBST). A control well containing only kinetic buffer
324 (PBST) was used for background measurement. The kinetic parameters and binding affinities
325 between the RBD-hFc and ACE2 were analyzed using Octet Data Analysis software 12.2.0.20 with
326 curve-fitting kinetic analysis.
327
328 **Pseudovirus production**
329 VSV-dG-based pseudovirus carrying spike proteins from various coronaviruses were produced
330 following a modified protocol as previously described[53]. Briefly, HEK293T cells were transfected

331 with plasmids expressing coronaviruses spike proteins. At 24 hours post-transfection, cells were
332 transduced with 1.5×10^6 $TCID_{50}$ VSV-G glycoprotein-deficient VSV expressing GFP and firefly
333 luciferase (VSV-dG-GFP-fLuc, constructed and produced in-house) diluted in DMEM with 8 μg/mL
334 polybrene for 4-6 hours at 37 °C. After three PBS washes, the culture medium was replenished with
335 either DMEM+10% FBS or SMM 293-TII Expression Medium (Sino Biological, M293TII), along
336 with an antibody (from I1-mouse hybridoma) targeting the VSV-glycoprotein to neutralize any
337 remaining VSV-dG-GFP-fLuc. Twenty-four hours later, the pseudovirus containing supernatant was
338 clarified through centrifugation at 12,000 rpm for 5 mins at 4°C, aliquoted, and stored at -80°C.
339
340 **Pseudovirus entry assay**
341 Pseudovirus entry assays were conducted using HEK293T cells transiently or stably expressing
342 different ACE2 orthologues. Typically, $3x10^4$ trypsinized cells were incubated with pseudovirus
343 (2×10^5 $TCID_{50}$/100 μL) in a 96-well plate to allow attachment and viral entry. Unless otherwise
344 specified, pseudoviruses were treated with 10 μg/mL TPCK-trypsin (Sigma-Aldrich, T8802)
345 before inoculation. Generally, pseudoviruses produced in serum-free SMM 293-TII Expression
346 Medium were incubated with TPCK-treated trypsin for 10 mins at room temperature, and the
347 proteolytic activity was neutralized by FBS in the culture medium for the cells. Intracellular
348 luciferase activity was measured using the Bright-Glo Luciferase Assay Kit (Promega, E2620) and
349 detected with a GloMax 20/20 Luminometer (Promega) at 18 hours post-infection.
350
351 **Western blot**
352
353 Cells expressing the indicated proteins were lysed in 1% TritonX/PBS+1 mM PMSF (Beyotime,
354 ST506) for 10 mins at 4°C. The lysate was clarified after centrifugation of 12,000 rpm for 5 mins at
355 4°C, and then incubated at 98°C for 10 mins after mixing with the 1/5 volume of 5×SDS loading
356 buffer. Following gel electrophoresis and membrane transfer, the membranes were blocked with 5%
357 skimmed milk in PBST for 2 hours at room temperature. Subsequently, the membrane was incubated
358 with 1 μg/mL anti-Flag mAb (Sigma, F1804) or anti-β-tubulin (Immmuno Way, YM3030) mAb
359 diluted in PBST containing 1% milk overnight at 4°C. After four washes with PBST, the blots were
360 incubated with Horseradish peroxidase (HRP)-conjugated secondary antibody AffiniPure Goat

361 Anti-Mouse in 1% skim milk diluted in PBST and incubated for one hour at room temperature.
362 Finally, the blots were washed four times again by PBST and visualized using an Omni-ECL Femto
363 Light Chemiluminescence Kit (EpiZyme, SQ201) through a ChemiDoc MP Imaging System
364 (Bio-Rad).
365
366 **Immunofluorescence assay**
367 Immunofluorescence assays were conducted to determine the expression levels of ACE2 orthologues
368 with C-terminal fused 3×Flag tags. Generally, the transfected cells were fixed and permeabilized by
369 incubation with 100% methanol for 10 mins at room temperature. Subsequently, the cells were
370 incubated with a mouse antibody M2 (Sigma-Aldrich, F1804) diluted in PBS/1% BSA for one hour
371 at 37℃. After a PBS wash, the cells were incubated with Alexa Fluor 594-conjugated goat
372 anti-mouse IgG (Thermo Fisher Scientific, A32742) secondary antibody diluted in 1% BSA/PBS for
373 one hour at 37℃. The images were captured and merged with a fluorescence microscope (Mshot,
374 MI52-N) after the nucleus was stained blue with Hoechst 33342 reagent (1:5,000 dilution in PBS).
375
376 **Bioinformatic and structural analysis**
377 Sequence alignments of different bats ACE2 were performed using either the MUSCLE algorithm by
378 MEGA-X (version 10.1.8) or ClustalW software (https://www.genome.jp/tools-bin/clustalw).
379 Phylogenetic trees were generated using the maximal likelihood method in IQ-TREE
380 (http://igtree.cibiv.univie.ac.at/) (1000 Bootstraps) and refined with iTOL (v6) (https://itol.embl.de/).
381 The structures of MOW-15-22, PnNL2018B, and HKU31 RBD were predicted using
382 alphaFold2.ipynb-Colaboratory. The structure of NeoCoV RBD & P.pip ACE2 complex (7WPO),
383 MERS-CoV RBD (4KR0), HKU4 RBD (4QZV), MOW-15-22 RBD, HKU31 RBD, and
384 PnNL2018B RBD were visualized and analyzed using the Chimera (V.1.14).
385
386 **Statistical Analysis**
387 Most experiments related to pseudovirus infection were conducted 2-3 times with 2-4 biological
388 repeats. Representative results were shown. Data were presented by MEAN±SD, as indicated in the
389 figure legends. Unpaired two-tailed t-tests were conducted for all statistical analyses using GraphPad
390 Prism 8. $P<0.05$ was considered significant. * $p<0.05$, ** $p<0.01$, *** $p<0.005$, and **** $p<0.001$.

Acknowledgements

This study was supported by the National Natural Science Foundation (NSFC) of China projects (82322041, 32270164, 32070160), Fundamental Research Funds for the Central Universities (2042023kf0191, 2042022kf1188), Hubei Provincial Natural Science Foundation (2023AFA015).

Author contributions

H.Y. conceptualized the study design. L.C., and C.B.M. performed the experiments. C.B.M., C.L, H.Y., and Q.X. analyzed the data. C.B.M., C.L, H.Y., and Q.X. interpreted the results. H.Y. and C.B.M. wrote the initial drafts of the manuscript. H.Y., C.B.M., and C.L, revised the manuscript. C.B.M., C.L, H.Y., Q.X., X.Y.,Y.M.C.,J.Y.S.,P.L.,F.T., and M.L.H. commented on the manuscript. All authors read and approved the final manuscript.

Competing interests

The authors declare no competing interests.

Data availability

The authors declare that all data supporting the findings of this study are available with the paper and its supplementary information files.

Figure legend

Figure1

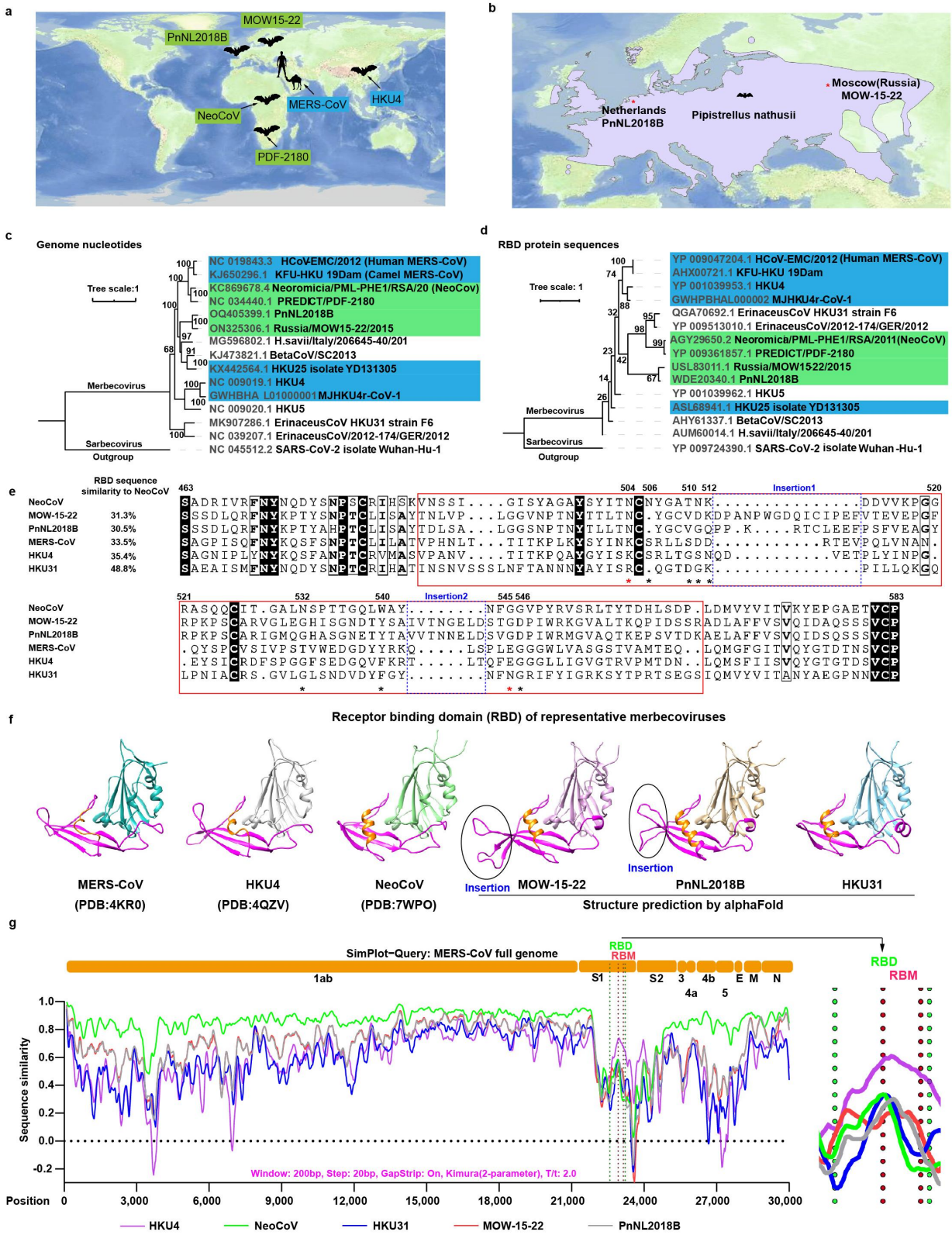

Fig.1 Analyses of MOW-15-22 and PnNL2018B RBD suggest potential ACE2 usage.

(a) Discovery locations and natural hosts of indicated merbecoviruses. Merbecoviruses that use DPP4 as their receptor are marked with a blue background, while those using ACE2 are highlighted

418 in green. **(b)** Geographical distribution of the *Pipistrelle nathusii* in Europe. The purple regions
419 represent its habitat, the data are retrived from the IUCN (International Union for Conservation of
420 Nature) Red List of Threatened Species, and the distribution chart is generated by Geoscene Pro. The
421 red arrows indicate the discovery location of MOW-15-22 and PnNL2018B.**(c-d)** Phylogenetic trees
422 of the representative merbecoviruses generated using complete genomes **(c)** or RBD protein
423 sequences **(d)** with the IQ-tree method. The background color distinguishes ACE2-using (green) and
424 DPP4-using (blue) merbecoviruses. The Sarbecovirus SARS-CoV-2 was set as the outgroup. **(e)** The
425 alignment of RBM sequences of indicated merbecoviruses generated using ClustalW and rendered
426 with ESPript. The putative receptor binding loops corresponding to NeoCoV RBM are highlighted in
427 a red dashed box, and two notable insertions in MOW-15-22 or PnNL2018B are indicated by the two
428 blue dashed boxes. Residues involved in crucial interactions between NeoCoV and P.pip ACE2 are
429 marked with asterisks, while conserved residues shared by NeoCoV, MOW-15-22, and PnNL2018B
430 are highlighted in red. **(f)** Cryo-EM Structures or AlphaFold-Predicted RBD structures of
431 representative merbecovirus. Pink indicates putative RBM, and orange represents the characterized
432 helix that may affect receptor usage. Two specific RBM insertions in MOW-15-22 and PnNL2018B
433 as mentioned in (e) are highlighted by blue circles. **(g)** Simplot analysis of the complete genome
434 nucleotide sequence similarity of five merbecoviruses analyzed based on the MERS-CoV genome.
435 Different ORF regions are indicated at the top. Green dashed lines mark RBD regions, and red
436 dashed lines mark RBM regions. The right panel represents the magnified charts of the RBD region.
437 T/t, transition/transversion ratio.
438
439

Figure2

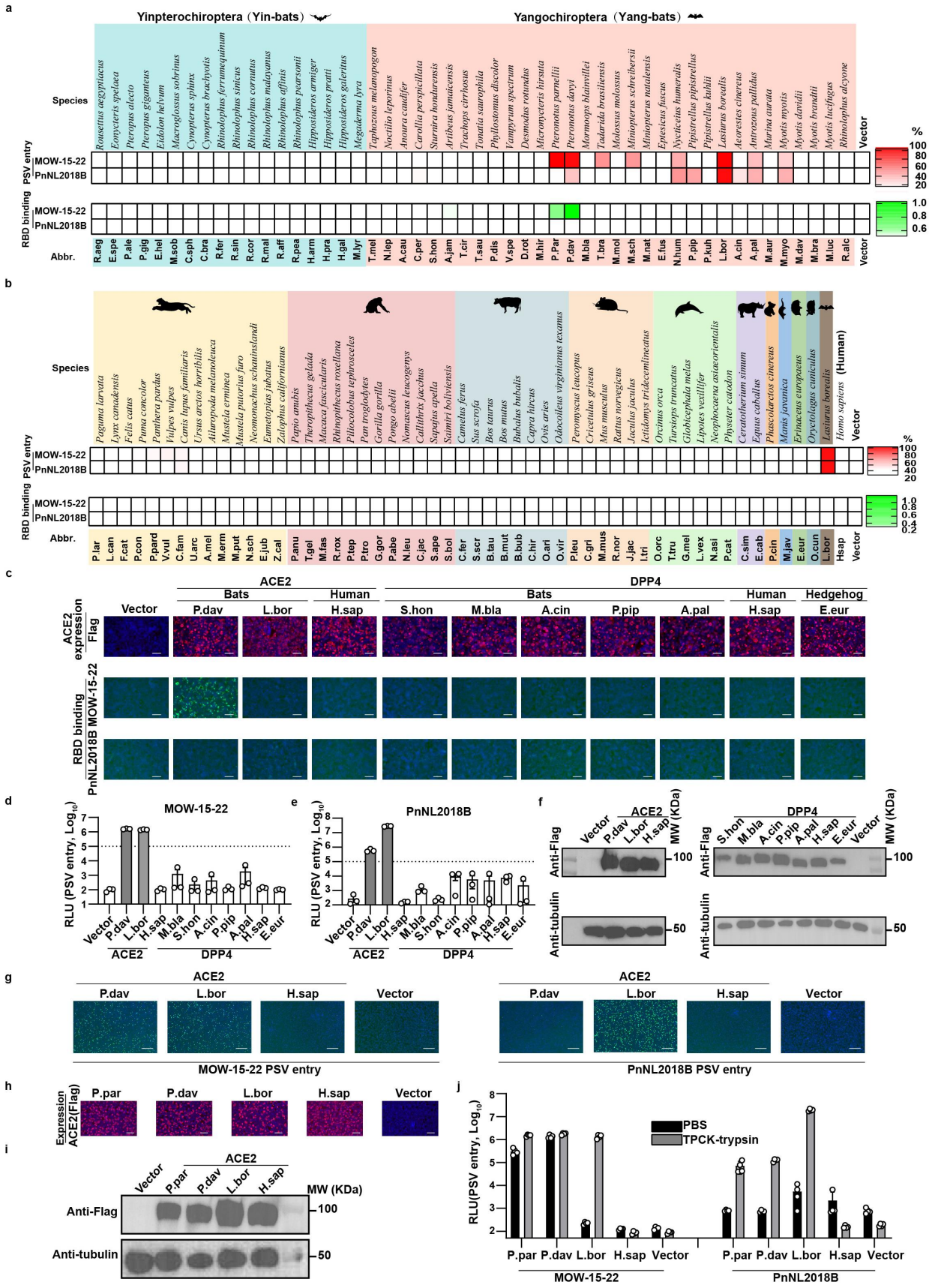

a
Yinpterochiroptera (Yin-bats)
Yangochiroptera (Yang-bats)
Species
PSV entry
RBD binding
MOW-15-22
PnNL2018B
Abbr.
Vector
%
b
Species
PSV entry
RBD binding
MOW-15-22
PnNL2018B
Abbr.
Vector
(Human)
c
ACE2
DPP4
Bats
Human
Hedgehog
Vector
P.dav
L.bor
H.sap
S.hon
M.bla
A.cin
P.pip
A.pal
E.eur
ACE2 expression
Flag
RBD binding
PnNL2018B MOW-15-22
d
MOW-15-22
RLU (PSV entry, Log10)
ACE2
DPP4
e
PnNL2018B
f
Anti-Flag
Anti-tubulin
MW (KDa)
g
ACE2
P.dav
L.bor
H.sap
Vector
MOW-15-22 PSV entry
PnNL2018B PSV entry
h
Expression ACE2(Flag)
P.par
i
Anti-Flag
Anti-tubulin
MW (KDa)
j
PBS
TPCK-trypsin
RLU(PSV entry, Log10)
MOW-15-22
PnNL2018B

440

Fig.2 MOW-15-22 and PnNL2018B can use several bats ACE2 orthologues for efficient viral entry.

(a-b) Heat map representing MOW-15-22 and PnNL2018B RBD binding and PSV entry in HEK293T cells transiently expressing the various ACE2 orthologues from bats (**a**) or other mammals (**b**). Above: species names; Below: species abbreviations. Yinpterochiroptera (Yin-bats) and Yangchiroptera (Yang-bats) are indicated with cyan and pink backgrounds, respectively. Different mammal orders are marked with colored backgrounds, from left to right: Carnivora, Primates, Artiodactyla, Rodentia, Cetacea, Perissodactyla, Diprotodontia, Pholidota, Erinaceomorpha, and Lagomorpha. RBD binding efficiency is represented as mean fluorescence values in RBD binding assays, and the entry efficiency is normalized to the percentage of RLU values of the ACE2 orthologue with the highest RLU. (**c**) Expression levels of representative ACE2 and DPP4 receptors and the corresponding MOW-15-22 and PnNL2018B RBD binding intensity indicated by live-cell immunofluorescence. **(d-e)** PSV entry efficiency of MOW-15-22 **(d)** and PnNL2018B **(e)** in HEK293T expressing the indicated receptors. **(f)** Western blot analysis of receptor expression levels detecting C-terminal fused flag tags. **(g)** PSV entry efficiency of MOW-15-22 and PnNL2018B in HEK293T cells stably expressing P.dav, P.par, L.bor, and H.sap ACE2, as indicated by GFP intensity. **(h-i)** Immunofluorescence (**h**) and Western blot (**i**) detecting the ACE2 C-terminal flag tags of the diffenent ACE2 orthologues. **(j)** The PSV entry efficiency of MOW-15-22 and PnNL2018B with or without the presence of 10 μ g/mL TPCK-treated trypsin.

Data are presented as mean for n=4 biologically independent cells for **a** and **b.** Data are presented as mean ± SD for n=3 (**d, e**) or n=4 (**j**) biologically independent cells. Data representative of two independent experiments. The scale bars represent 100 μm for **c** and **g.** RLU: relative luciferase unit.

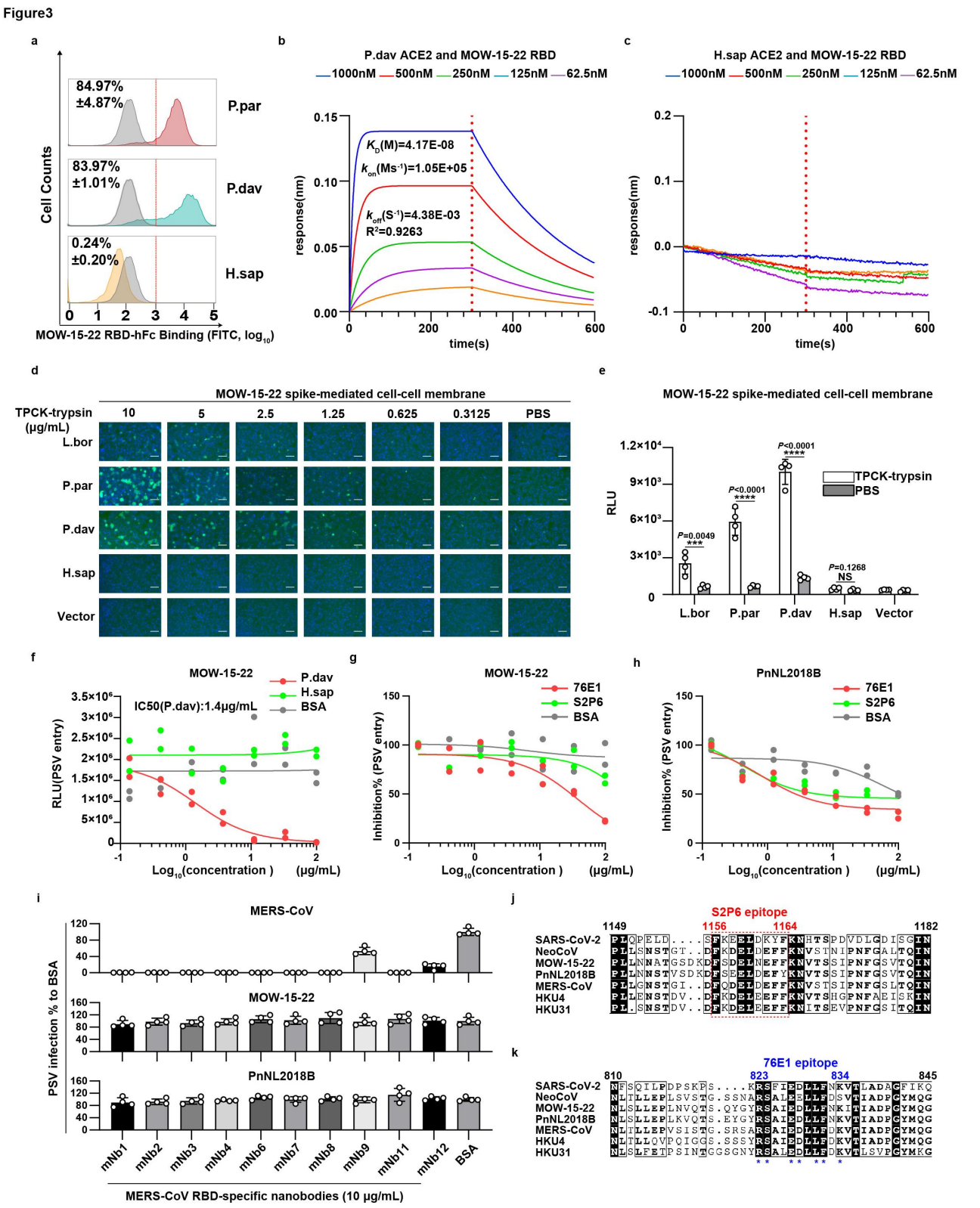

464

465 **Fig. 3 Characterization of MOW-15-22 RBD binding, fusion, and viral entry mediated by bat**

466 **ACE2.**

467 （**a**）Flow cytometry analysis of MOW15-22 RBD-hFc binding with HEK293T cells transiently

468 expressing the indicated ACE2 orthologues. The red dashed lines represent the threshold for positive

469 cells based on vector control. The positive ratio of the hFc staining signal is presented as Mean±SD.
470 (**b-c**) Binding kinetics between MOW-15-22 RBD-hFc and the soluble recombinant P.dav **(b)** or
471 H.sap **(c)** ACE2 ectodomain proteins analyzed by BLI assays. (**d-e**) MOW-15-22 spike mediated
472 cell-cell membrane fusion in HEK293T stably expressing ACE2 orthologues in the presence of
473 different concentration of TPCK-treated trypsin (two-fold serial-dilution from 10 μg/ml). Cell fusion
474 efficiency is indicated by eGFP intensity (**d**) and live-cell Renilla luciferase activity (**e**) through the
475 reconstitution of dual-split reporter proteins (DSP). (**f**) Dose-dependent inhibition of MOW-15-22
476 S-mediated entry by soluble ACE2 in HEK293T cells stably expressing P.dav ACE2. (**g-h**) Inhibitory
477 activity of broadly neutralizing antibodies 76E1 and S2P6 against MOW-15-22 **(g)** and PnNL2018B
478 **(h)** S pseudotyped viruses. **(i)** Inhibitory activity of MERS-CoV specific nanobodies (10 μ g/mL)
479 against MERS-CoV, MOW-15-22 and PnNL2018B PSV entry. **(j-k)** Sequence alignment displaying
480 the corresponding sequences of S2P6 **(j)** and 76E1 **(k)** epitopes in indicated coronavirus spikes. The
481 red dashed box indicates the key epitope sequences of S2P6, and the blue asterisks indicate the key
482 amino acid for 76E1 recognition. The numbering is based on SARS-CoV-2 spike sequences.
483 Data are presented as mean ± SD for n=3 biologically independent cells for **e** and n=4 **for i.** Data are
484 shown as n=2 biologically independent cells for **f, g,** and **h.** Data representative of two independent
485 experiments for **a-i.** RLU: relative light unit. The scale bars represent 100 μ m for **d**.
486

Figure4

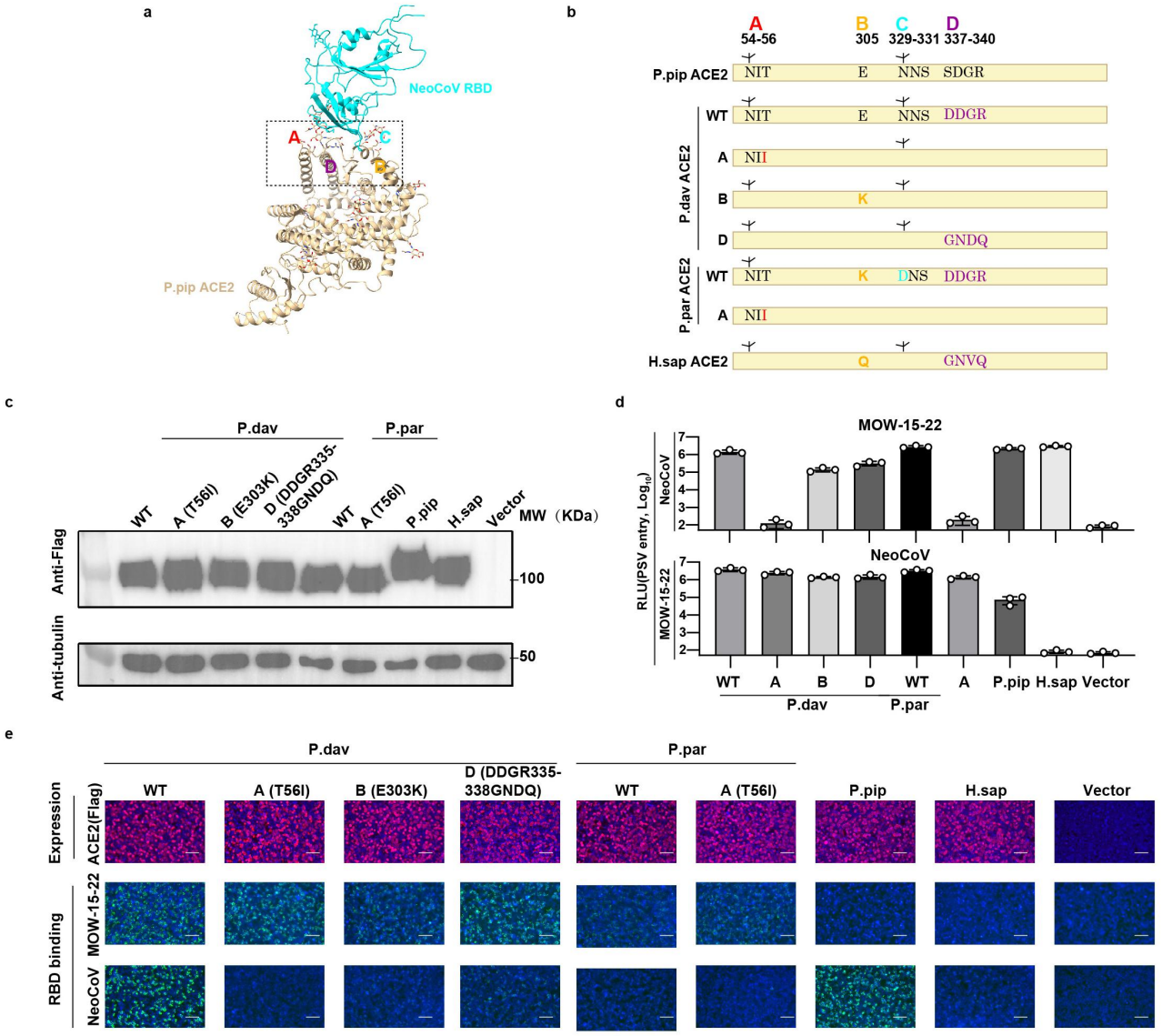

Fig. 4 MOW-15-22 utilizes a distinct glycan-independent binding mode to recognize ACE2 compared with NeoCoV.

(a) Structural view of four host range determinants (A-D) critical for species-specific ACE2 recognition by NeoCoV. **(b)** Schematic illustration of P.dav or P.par ACE2 mutants with indicated determinants replaced by Ppip ACE2 counterparts. The glycosylation sites in determinants A and C are demonstrated. **(c)** Western blot analyzing the expression of indicated WT and mutated ACE2 in HEK293T cells. **(d-e)** MOW-15-22 and NeoCoV PSV entry (d) and RBD binding efficiency(e) in HEK293T transiently expressing the indicated WT or mutants ACE2 orthologues. The expression level of the indicated ACE2 orthologues was verified by immunofluorescence (e, upper).

Data are presented as mean ± SD for n=3 biologically independent cells for **d.** Data representative of

498 two independent experiments for **c-e.** RLU: relative luciferase unit. Mw: molecular weight. The scale
499 bars represent 100 μm for **e**.
500
501
502

503 1. Li, W. *et al.* Bats are natural reservoirs of SARS-like coronaviruses. *Science* **310**, 676-679 (2005).
504 2. Ge, X.Y. *et al.* Isolation and characterization of a bat SARS-like coronavirus that uses the ACE2 receptor. *Nature*
505 **503**, 535-538 (2013).
506 3. Wang, Q. *et al.* Bat origins of MERS-CoV supported by bat coronavirus HKU4 usage of human receptor CD26.
507 *Cell Host Microbe* **16**, 328-337 (2014).
508 4. Wong, A.C.P., Li, X., Lau, S.K.P. & Woo, P.C.Y. Global Epidemiology of Bat Coronaviruses. *Viruses* **11**, 174 (2019).
509 5. Zhou, P. *et al.* A pneumonia outbreak associated with a new coronavirus of probable bat origin. *Nature* **579**,
510 270-273 (2020).
511 6. Chen, L. *et al.* RNA based mNGS approach identifies a novel human coronavirus from two individual pneumonia
512 cases in 2019 Wuhan outbreak. *Emerg Microbes Infect* **9**, 313-319 (2020).
513 7. Latinne, A. *et al.* Origin and cross-species transmission of bat coronaviruses in China. *Nat Commun* **11**, 4235
514 (2020).
515 8. Temmam, S. *et al.* Bat coronaviruses related to SARS-CoV-2 and infectious for human cells. *Nature* **604**, 330-336
516 (2022).
517 9. Ksiazek, T.G. *et al.* A novel coronavirus associated with severe acute respiratory syndrome. *N Engl J Med* **348**,
518 1953-1966 (2003).
519 10. Zaki, A.M., van Boheemen, S., Bestebroer, T.M., Osterhaus, A.D. & Fouchier, R.A. Isolation of a novel
520 coronavirus from a man with pneumonia in Saudi Arabia. *N Engl J Med* **367**, 1814-1820 (2012).
521 11. WHO. MERS situation update; https://www.emro.who.int/health-topics/mers-cov/mers-outbreaks.html (2023).
522 12. Alagaili, A.N. *et al.* Middle East respiratory syndrome coronavirus infection in dromedary camels in Saudi Arabia.
523 *mBio* **5**, e00884-14 (2014).
524 13. Meyer, B. *et al.* Antibodies against MERS coronavirus in dromedary camels, United Arab Emirates, 2003 and
525 2013. *Emerg Infect Dis* **20**, 552-9 (2014).
526 14. Memish, Z.A. *et al.* Human infection with MERS coronavirus after exposure to infected camels, Saudi Arabia,
527 2013. *Emerg Infect Dis* **20**, 1012-5 (2014).
528 15. Azhar, E.I. *et al.* Evidence for camel-to-human transmission of MERS coronavirus. *N Engl J Med* **370**, 2499-505
529 (2014).
530 16. Mohd, H.A., Al-Tawfiq, J.A. & Memish, Z.A. Middle East Respiratory Syndrome Coronavirus (MERS-CoV) origin
531 and animal reservoir. *Virol J* **13**, 87 (2016).
532 17. Hassan, M.M. *et al.* NeoCoV Is Closer to MERS-CoV than SARS-CoV. *Infect Dis (Auckl)* **13**, 1178633720930711
533 (2020).
534 18. Lu, G., Wang, Q. & Gao, G.F. Bat-to-human: spike features determining 'host jump' of coronaviruses SARS-CoV,
535 MERS-CoV, and beyond. *Trends Microbiol* **23**, 468-78 (2015).
536 19. Li, F. Structure, Function, and Evolution of Coronavirus Spike Proteins. *Annu Rev Virol* **3**, 237-261 (2016).
537 20. Maginnis, M.S. Virus-Receptor Interactions: The Key to Cellular Invasion. *J Mol Biol* **430**, 2590-2611 (2018).
538 21. Wan, Y., Shang, J., Graham, R., Baric, R.S. & Li, F. Receptor Recognition by the Novel Coronavirus from Wuhan:
539 an Analysis Based on Decade-Long Structural Studies of SARS Coronavirus. *J Virol* **94**, e00127-20 (2020).

22. Li, F. Receptor recognition mechanisms of coronaviruses: a decade of structural studies. *J Virol* **89**, 1954-1964 (2015).
23. Tortorici, M.A. & Veesler, D. Structural insights into coronavirus entry. *Adv Virus Res* **105**, 93-116 (2019).
24. Li, W. *et al.* Angiotensin-converting enzyme 2 is a functional receptor for the SARS coronavirus. *Nature* **426**, 450-454 (2003).
25. Hofmann, H. *et al.* Human coronavirus NL63 employs the severe acute respiratory syndrome coronavirus receptor for cellular entry. *Proc Natl Acad Sci U S A* **102**, 7988-7993 (2005).
26. Ithete, N.L. *et al.* Close relative of human Middle East respiratory syndrome coronavirus in bat, South Africa. *Emerg Infect Dis* **19**, 1697-1699 (2013).
27. Corman, V.M. *et al.* Rooting the phylogenetic tree of middle East respiratory syndrome coronavirus by characterization of a conspecific virus from an African bat. *J Virol* **88**, 11297-11303 (2014).
28. Anthony, S.J. *et al.* Further Evidence for Bats as the Evolutionary Source of Middle East Respiratory Syndrome Coronavirus. *mBio* **8**, e00373-17 (2017).
29. Lau, S.K.P. *et al.* Identification of a Novel Betacoronavirus (Merbecovirus) in Amur Hedgehogs from China. *Viruses* **11**, 980 (2019).
30. Liu, K. *et al.* Binding and molecular basis of the bat coronavirus RaTG13 virus to ACE2 in humans and other species. *Cell* **184**, 3438-3451.e10 (2021).
31. (!!! INVALID CITATION !!!).
32. Xiong, Q. *et al.* Close relatives of MERS-CoV in bats use ACE2 as their functional receptors. *Nature* **612**, 748-757 (2022).
33. Ma, C. *et al.* Broad host tropism of ACE2-using MERS-related coronaviruses and determinants restricting viral recognition. *Cell Discov* **9**, 57 (2023).
34. Woo, P.C., Lau, S.K., Li, K.S., Tsang, A.K. & Yuen, K.Y. Genetic relatedness of the novel human group C betacoronavirus to Tylonycteris bat coronavirus HKU4 and Pipistrellus bat coronavirus HKU5. *Emerg Microbes Infect* **1**, e35 (2012).
35. Speranskaya, A.S. *et al.* Identification and Genetic Characterization of MERS-Related Coronavirus Isolated from Nathusius' Pipistrelle (Pipistrellus nathusii) near Zvenigorod (Moscow Region, Russia). *Int J Environ Res Public Health* **20**(2023).
36. Mols, V.C. *et al.* Intestinal Tropism of a Betacoronavirus (Merbecovirus) in Nathusius's Pipistrelle Bat (Pipistrellus nathusii), Its Natural Host. *J Virol* **97**, e0009923 (2023).
37. Reusken, C.B. *et al.* Circulation of group 2 coronaviruses in a bat species common to urban areas in Western Europe. *Vector Borne Zoonotic Dis* **10**, 785-91 (2010).
38. Iucnredlist.Org Available online: https://www.iucnredlist.org/species/17316/22132621.
39. Eurobats.Org Available online: https://www.eurobats.org/About_eurobats/Protected_bat_species/Pipistrellus_nathusii.
40. Moreno, A. *et al.* Detection and full genome characterization of two beta CoV viruses related to Middle East respiratory syndrome from bats in Italy. *Virol J* **14**, 239 (2017).
41. Yan, H. *et al.* ACE2 receptor usage reveals variation in susceptibility to SARS-CoV and SARS-CoV-2 infection among bat species. *Nat Ecol Evol* **5**, 600-608 (2021).
42. Menachery, V.D. *et al.* Trypsin Treatment Unlocks Barrier for Zoonotic Bat Coronavirus Infection. *J Virol* **94**(2020).
43. Pinto, D. *et al.* Broad betacoronavirus neutralization by a stem helix-specific human antibody. *Science* **373**, 1109-1116 (2021).
44. Sun, X. *et al.* Neutralization mechanism of a human antibody with pan-coronavirus reactivity including

584 SARS-CoV-2. *Nat Microbiol* **7**, 1063-1074 (2022).
585 45. Millet, J.K., Jaimes, J.A. & Whittaker, G.R. Molecular diversity of coronavirus host cell entry receptors. *FEMS*
586 *Microbiol Rev* **45**(2021).
587 46. Tortorici, M.A. *et al.* Structure, receptor recognition, and antigenicity of the human coronavirus
588 CCoV-HuPn-2018 spike glycoprotein. *Cell* **185**, 2279-2291.e17 (2022).
589 47. Yeager, C.L. *et al.* Human aminopeptidase N is a receptor for human coronavirus 229E. *Nature* **357**, 420-2
590 (1992).
591 48. Tresnan, D.B., Levis, R. & Holmes, K.V. Feline aminopeptidase N serves as a receptor for feline, canine, porcine,
592 and human coronaviruses in serogroup I. *J Virol* **70**, 8669-74 (1996).
593 49. Li, W. *et al.* Broad receptor engagement of an emerging global coronavirus may potentiate its diverse
594 cross-species transmissibility. *Proc Natl Acad Sci U S A* **115**, E5135-E5143 (2018).
595 50. Cameroni, E. *et al.* Broadly neutralizing antibodies overcome SARS-CoV-2 Omicron antigenic shift. *Nature* **602**,
596 664-670 (2022).
597 51. McCallum, M. *et al.* Structural basis of SARS-CoV-2 Omicron immune evasion and receptor engagement.
598 *Science* **375**, 864-868 (2022).
599 52. Corman, V.M. *et al.* Characterization of a novel betacoronavirus related to middle East respiratory syndrome
600 coronavirus in European hedgehogs. *J Virol* **88**, 717-724 (2014).
601 53. Whitt, M.A. Generation of VSV pseudotypes using recombinant DeltaG-VSV for studies on virus entry,
602 identification of entry inhibitors, and immune responses to vaccines. *J Virol Methods* **169**, 365-374 (2010).

603